Yb-doped yttrium aluminum perovskite for radiation balanced laser application

Nakayama, Yuta

Harada, Yukihiro

Kita, Takashi

(Citation)
Proceedings Volume 11702, Photonic Heat Engines: Science and Applications III,11702:117020K

(Issue Date)
2021-04-01

(Resource Type)
conference paper

(Version)
Version of Record

(URL)
https://hdl.handle.net/20.500.14094/0100477743

Yb-doped yttrium aluminum perovskite for radiation balanced laser application

Nakayama, Yuta, Harada, Yukihiro, KIta, Takashi

Yuta Nakayama, Yukihiro Harada, Takashi KIta, "Yb-doped yttrium aluminum perovskite for radiation balanced laser application," Proc. SPIE 11702, Photonic Heat Engines: Science and Applications III, 117020K (1 April 2021); doi: 10.1117/12.2577115

SPIE.

Event: SPIE OPTO, 2021, Online Only

Yb-doped Yttrium Aluminum Perovskite for Radiation Balanced Laser Application

Yuta Nakayama *, Yukihiro Harada, and Takashi Kita
Kobe University, 1–1 Rokko-dai, Nada ward, Kobe, Japan 657-8501

ABSTRACT

Radiation balanced laser (RBL) can be realized by managing the cooling process via the anti-Stokes photoluminescence (PL), the small-signal gain, and the heating processes including the Stokes shifts and the multi-phonon relaxation. Yttrium aluminum perovskite (YAP) shows lower phonon energy than yttrium aluminum garnet (YAG) which the radiation balanced laser was demonstrated. According to the single-frequency phonon model, the low maximum phonon energy of YAP makes the multi-phonon relaxation probability of Yb-doped YAP [(Yb:Y)AP] smaller than Yb-doped YAG [(Yb:Y)AG]. The low multi-phonon relaxation probability of YAP suggests that (Yb:Y)AP is suitable material for RBL. In this work, we evaluated the PL characteristics and estimated the ideal laser cooling efficiency and the small-signal gain of the (Yb:Y)AP ($Yb_{0.1}Y_{0.9}AlO_3$) ceramics fabricated by a solid-state reaction method. We used McCumber's relationship and referred to the literatures to derive the absorption and the small-signal gain spectra. The fluorescence re-absorption is observed in the PL spectra of (Yb:Y)AP ceramics with a thickness of ~2 mm, whereas the re-absorption is not observed in (Yb:Y)AG ($Yb_{0.3}Y_{2.7}Al_5O_{12}$). This result indicates the strong absorbance of (Yb:Y)AP. The obtained ideal laser cooling efficiencies of (Yb:Y)AP and (Yb:Y)AG at 300 K were 1.4 and 1.8%, respectively. On the other hand, the maximum small-signal gain of 0.27 cm^{-1} in (Yb:Y)AP is 3.5 times larger than that of 0.078 cm^{-1} in (Yb:Y)AG. The large small-signal gain of (Yb:Y)AP arises from its strong absorbance and intrinsic energy structure.

Keywords: photonic heat engines, radiation balanced laser, laser cooling in solids, anti-Stokes PL, rare-earth, oxides, perovskite

1. INTRODUCTION

Irradiation of laser light on an emissive matter and extraction of anti-Stokes photoluminescence (PL) via an absorption process of thermal energy can refrigerate the material itself[1] if the heat simultaneously generated in the material is enough smaller than the laser cooling power. Therefore, suppression of the heating process is the highest priority to achieve net cooling (an actual temperature dropping of matter). As for laser cooling in a solid-state material, the challenging research in Nd-doped yttrium aluminum garnet (Nd:YAG) suggested that the main heat sources are an unexpected impurity and the multi-phonon relaxation process[2]. The transition metals were determined as the critical impurities[3] and the purification of raw materials significantly improved the minimum attainable temperature below 100 K[4] in Yb-doped yttrium lithium fluoride (Yb:YLF) showing low-phonon energy. Nowadays, utilizing Yb:YLF and Yb-doped yttrium aluminum garnet (Yb:YAG), the all-solid-state optical cryocooler and the radiation balanced laser applications have been demonstrated for the first time[5,6].

There are several material systems that have been intensively investigated until the present. III-V group semiconductor, the lead-halide perovskite, and a rare-earth (RE)-doped material are well-known laser cooling material candidates. The expected attainable temperature of semiconductors is ~10 K which is much lower than RE-doped material[7]. However, a high refractive index of III-V group semiconductor prevents an escape of anti-Stokes PL from material which is a possible origin of a heat generation by re-absorption process and non-radiative recombination. Because the non-radiative recombination between bandgap causes much larger heat than the dissipated thermal energy by anti-Stokes PL, it requires an external quantum efficiency (EQE) nearly unity. On contrary, a lead-halide perovskite material, especially $CsPbBr_3$ nanocrystals shows an extremely high quantum efficiency of ~99%[8]. The first demonstration of net cooling in $CsPbBr_3$ has been anticipated with the optical thermometry[9] which is available for material with temperature insensitive energy gap and nanostructure.

The RE-doped materials have been considered as better candidates as cooling material due to their narrow spectral linewidth and high internal quantum efficiency, and net cooling has been reported in various combinations of RE elements

Photonic Heat Engines: Science and Applications III, edited by Denis V. Seletskiy, Mansoor Sheik-Bahae, Masaru K. Kuno, Proc. of SPIE Vol. 11702, 117020K
 · doi: 10.1117/12.2577115

and host materials. As mentioned above, one of the hurdles to achieving net cooling in a RE-doped material is purification, and another is the design of material to minimize the multi-phonon relaxation. The multi-phonon relaxation probability W_{mp} for RE-doped material under the single-frequency model is written as follows[10,11]:

$$W_{mp} = B\left(\frac{\exp\left(\frac{E_p}{k_B T}\right)}{\exp\left(\frac{E_p}{k_B T}\right) - 1}\right)^N \exp(-\alpha \Delta E), \quad (1)$$

$$N = \frac{\Delta E}{E_p}, \quad (2)$$

$$\alpha = -\frac{\ln(G)}{E_p}, \quad (3)$$

where B is the spontaneous non-radiative decay rate (constant), E_p is the phonon energy, k_B is the Boltzmann constant, T is the absolute temperature, ΔE is the energy difference between two energy levels, and $N=\Delta E/E_p$ is the number of phonons involved. The host-dependent parameter α is defined as $-\ln(G)/E_p$, where G is the electron-phonon coupling constant. It has been shown that $-\ln(c)$ is usually almost constant (~3.5)[12]. As equation (1) shows that the multi-phonon relaxation probability follows the second term of Equation (1) to the power of the phonon number created N, a host material with high phonon energy would result in a high multi-phonon relaxation probability of the RE-doped laser cooling material. In the same way, as the multi-phonon relaxation probability exponentially decreases with an increasing energy gap ΔE, a RE-dopant showing a large energy gap between ground states and excited states suppress the heating process by the multi-phonon relaxation. The availability of these conclusions has been experimentally proved by the diverse previous works. For example, in the case of Yb:YLF which is a better material for a cryogenic laser cooling, the maximum phonon energy of ~440 cm^{-1} [13] is 23 times (=N) smaller than the ΔE of Yb^{3+} ~10000 cm^{-1} [14], therefore the multi-phonon relaxation rate of Yb:YLF is negligible compared with the radiative relaxation rate.

A radiation balanced laser (RBL) is one of the applications utilizing laser cooling in solids which can overcome the heat degradation of a laser device itself occurring in conventional laser light sources[15]. At the radiation balanced point, the temperature change of the system is zero because a generated heat in the RBL material by Stokes-shift is eliminated by the anti-Stokes PL cooling process at the same time. An oxide material is considered a better candidate for a high output power RBL because of the durability, high thermal conductivity, and chemical stability compared with fluorides. The first demonstration of RBL has been succeeded with Yb-doped yttrium aluminum garnet (Yb:YAG)[6] which is the Yb-doped crystal optically refrigerated for the first time[16].

2. METHODOLOGY

Hereafter, Yb:YAP is abbreviated as (Yb:Y)AP to clearly indicate that the Y ion was nominally replaced by Yb ion. In the same way, Yb:YAG is abbreviated as (Yb:Y)AG. The (Yb:Y)AG and (Yb:Y)AP ceramic samples for this work were fabricated by the solid-state reaction method. The Yb-doping concentration for both samples was a molar ratio of 0.1. Thus, the chemical formulas of (Yb:Y)AG and (Yb:Y)AP are $(Yb_{0.1}Y_{0.9})_3Al_5O_{12}$ and $(Yb_{0.1}Y_{0.9})AlO_3$, respectively. First, the high-purity (99.99%) raw materials (i.e., Yb_2O_3, Y_2O_3, and Al_2O_3) were mixed by ball milling for 1 hour. Then, a pressure of 200 MPa was applied to the mixed powder in a disc-shaped metal mold by oil press. After annealing in an electric furnace at 1000℃ for 10h, the obtained thick ceramic sample was polished to remove contaminations at the surface. The thickness of the polished ceramic sample is 2 mm. For the preparation of thin ceramic disks (thickness: approximately 100 μm), an additional mechanical polishing was performed. A laser diode operating at 405 nm was used for the PL measurement under indirect excitation via ET from Yb^{2+} to Yb^{3+} [20]. For the anti-Stokes PL and PLE imaging, a supercontinuum white laser light source was passed through a double monochromator and the obtained monochromated light was irradiated on the samples. PL signals from samples were dispersed by a single monochromator (F-number: 3.88, grating with 600 gr/mm and a blaze wavelength of 1000 nm) and detected by an InGaAs diode array with a thermoelectric cooler.

The ideal laser cooling efficiency η_c^{ideal} written in equation (4)[21] was calculated from the PLE image data which contains all signals of anti-Stokes PL, Stokes PL, and the excitation laser light. Where λ_{exc} is the excitation wavelength, λ_f is the mean fluorescence wavelength. At first, the excitation laser light signals were eliminated with a Gaussian fitting, and then the mean fluorescence wavelength was calculated from equation (5). Where $F(\lambda)$ is the fluorescence intensity.

$$\eta_c^{ideal} = \frac{\lambda_{exc}}{\lambda_f} - 1, \tag{4}$$

$$\lambda_f = \frac{\int \lambda F(\lambda) d\lambda}{\int F(\lambda) d\lambda}. \tag{5}$$

In addition to the ideal cooling efficiency, the gain of each materials working as RBL was also calculated by equation (6) written as follow[6]:

$$\gamma = \alpha_0(\lambda) \frac{i_P \left(\frac{\beta_P}{\beta_L} - 1\right) - 1}{1 + i_P + i_L}, \tag{6}$$

where α_0 is the absorption spectrum, $i_P = I_P/I_{SP}$ is the normalized pump intensity, $i_L = I_L/I_{SL}$ is the normalized laser intensity. I_P and I_L are the pump and laser intensities, respectively, and I_{SP} and I_{SL} are the saturation intensities of I_P and I_L, $\beta_P = [1+(Z_1/Z_2)\exp((E_{15}-hc/\lambda_P)/k_BT))]^{-1}$ and $\beta_L = [1+(Z_1/Z_2)\exp((E_{15}-hc/\lambda)/k_BT))]^{-1}$ are the fractions of cross-section reflecting the intrinsic energy structure of the material, Z_1 and Z_2 are the partition functions of lower and upper manifolds, E_{15} is the energy gap between E1 and E5 levels, λ_P is the pump wavelength.

3. RESULTS & DISCUSSION

Figure 1 shows the PL spectra of (Yb:Y)AP ceramics in different thicknesses of ~100 μm (top) and ~2 mm (bottom), excited by an indirect excitation process via charge transfer process from Yb^{2+} to Yb^{3+}. The vertical arrows and insert figure show the representative radiative processes found in the observed spectra. An asterisk mark indicates the unexpected peak signals originated by Yb^{3+} coordinated by other site symmetry such as Y site of yttrium aluminum monoclinic (YAM) and YAG.

The PL spectrum of (Yb:Y)AP thin ceramics (thickness of ~100 μm) shows narrow peaks corresponding to the *f-f* intra-orbital transitions of Yb^{3+} ion. On the other hand, the PL spectrum of (Yb:Y)AP thick ceramics (thickness of ~ 2 mm) is quenched and broadened from the (Yb:Y)AP thin ceramics. The strong re-absorption effect of (Yb:Y)AP is considered as the origin of the spectrum broadening in thick ceramics. From the reciprocal relationship between absorption and luminescence, the emitted luminescence signals in a short wavelength region can be easily trapped by other ions in the sample compared with luminescence in the long-wavelength region. Due to this re-absorption effect, the mean fluorescence

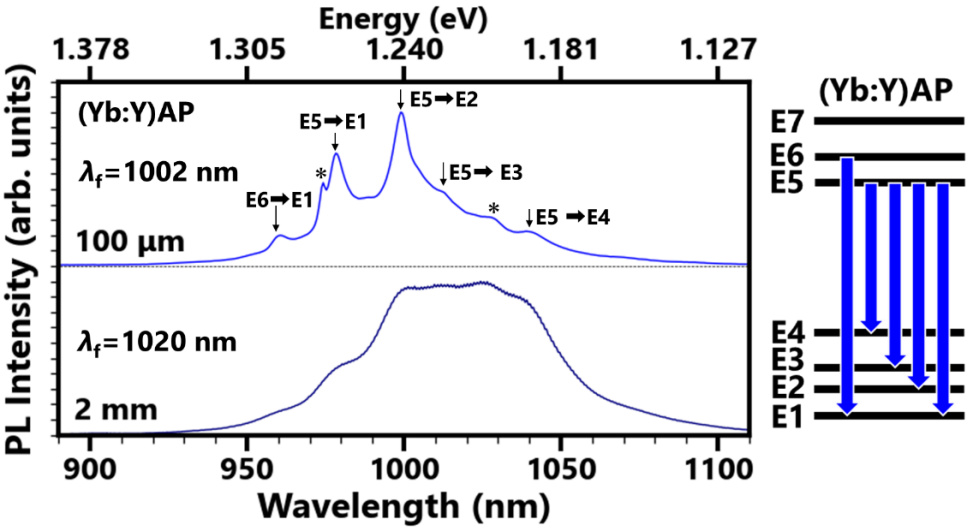

Figure 1 PL spectra of the (Yb:Y)AP in different thicknesses of 100 μm and ~2 mm. under indirect excitation at 405 nm. The vertical arrows and insert figure show the representative radiative processes found in the observed spectra. An asterisk mark indicates the unexpected peak signals originated by Yb^{3+} coordinated by other site symmetry such as Y site of yttrium aluminum monoclinic (YAM).

wavelength λ_f of thick ceramics red-shifted by 18 nm from that of thin ceramics. Additionally, in (Yb:Y)AG, a spectrum broadening by the thickness differences is not significant as observed in (Yb:Y)AP. The large spectrum broadening in (Yb:Y)AG despite their doping concentration is the same suggests the stronger light absorbance of Yb^{3+} in Y site of YAP than that of (Yb:Y)AG and well coincides with the reported optical properties of Yb:YAG and Yb:YAP[22].

To evaluate the ideal cooling efficiency and the relative cooling power of (Yb:Y)AP thin ceramics under the direct excitation by a spectroscopic way, the anti-Stokes PL and Stokes PL signals were measured all together as a function of an excitation wavelength. Figure 2 (a) shows the anti-Stokes PL spectrum of (Yb:Y)AP thin ceramics resonantly excited at 1018 nm (E4→E6) and the diagram presenting the excitation and observed anti-Stokes PL processes. The anti-Stokes PL peak signals at 952 (E7→E2), 960 (E6→E1), 979 (E5→E1), 999 (E5→E2), and 1012 (E5→E3) nm were observed. The small peak signal at 1064 nm is originated by the seed light source of supercontinuum light used for the direct excitation. Figure 2 (b) is the PLE image of (Yb:Y)AP at room temperature in the excitation wavelength region of 980~1030 nm. The horizontal axis, the vertical axis, and the color bar indicate the detected wavelength, the excitation wavelength, and the spectral intensities, respectively. The saturated signal in the PLE image is the excitation light scattered at a sample surface. Based on the PLE image of (Yb:Y)AP, the ideal cooling efficiency and the relative cooling power were calculated. By removing the excitation light signals in measured spectra with a Gaussian fitting, the fluorescence signal $F(\lambda)$ was obtained.

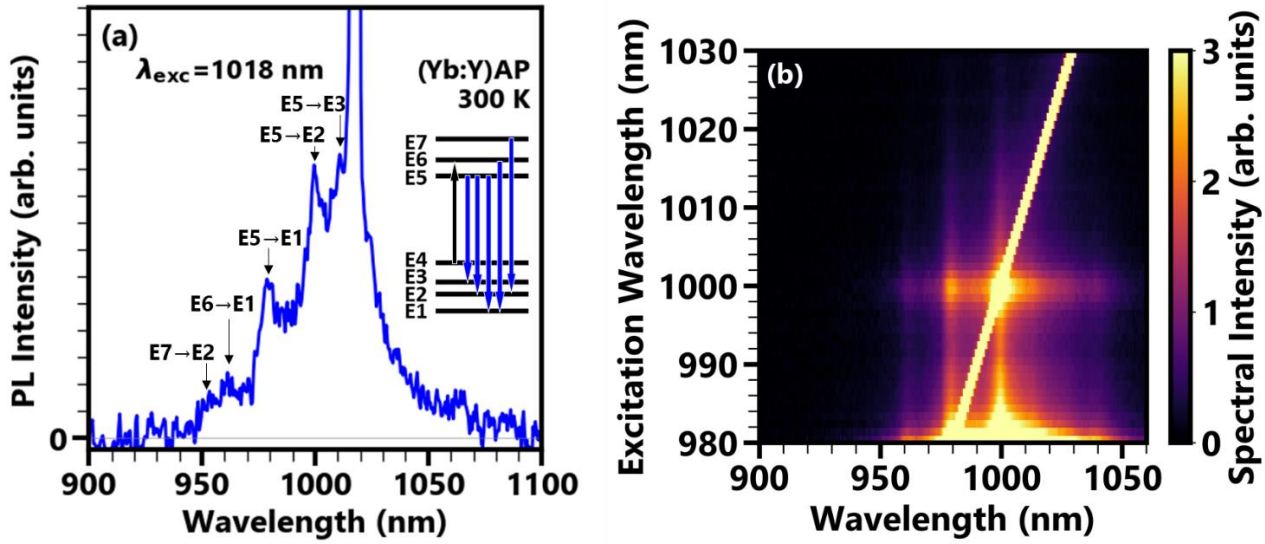

Figure 2 (a) PL spectrum of (Yb:Y)AP ceramics excited at 1018 nm, (b) PL excitation (PLE) image of the (Yb:Y)AP at room temperature. The horizontal axis, the vertical axis, and the color bar indicate the detected wavelength, the excitation wavelength, and the spectral intensities, respectively. The saturated signal in the PLE image is the excitation light scattered at the sample surface.

Figure 3 (a, b) present the calculation results of the ideal cooling efficiency and the relative laser cooling power[23] as a function of excitation wavelength in (Yb:Y)AP and (Yb:Y)AG. Blue diamond and white inverse triangle indicate the ideal cooling efficiency and relative cooling power in (Yb:Y)AP and (Yb:Y)AG, respectively. In Fig. 3(b), the blue filled region indicates where the cooling is possible. The relative cooling power is the relative value that is equivalent to the external quantum efficiency. For a more detailed derivation of the relative cooling power, please see the literature[23]. The comparable maximum ideal cooling efficiencies of ~1.5% in (Yb:Y)AP and ~1.8% in (Yb:Y)AG are consistent with the predicted performances in Yb-doped hosts[24]. The maximum cooling efficiency of RE-doped materials can be predicted from the energy structure of the cooling center. On the other hand, the relative cooling power reflects the photon numbers of extracted anti-Stokes PL and Stokes PL so that the optimum excitation condition to maximize the cooling power can be estimated from the spectrum. From Fig. 3(b), at 1018 nm excitation, the spectrum shows the maximum relative cooling power of (Yb:Y)AP. In the same way, the maximum relative cooling power of (Yb:Y)AG has been obtained at the excitation wavelength 1030 nm. The excitation 1030 nm in (Yb:Y)AG coincides with the result of the net cooling experiment[16]. Thus, 1018 nm is considered as the optimum pump wavelength for the laser cooling of (Yb:Y)AP.

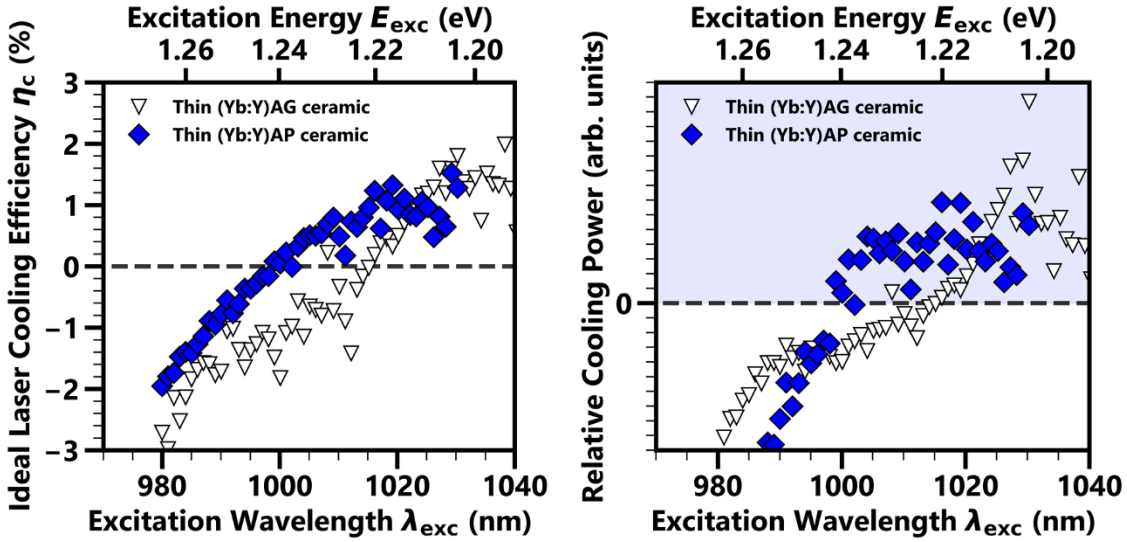

Figure 3 (a) The excitation energy dependence of the ideal cooling efficiency and (b) the relative laser cooling power[23] in (Yb:Y)AP and (Yb:Y)AG. Blue diamond and white inverse triangle indicate the performance parameters of (Yb:Y)AP and (Yb:Y)AG, respectively. (b) The blue filled region indicates where cooling is possible. The relative cooling power is the relative value that is equivalent to the external quantum efficiency. For a more detailed derivation of the relative cooling power, please see the literature[23].

Although the ideal cooling efficiency of (Yb:Y)AP is similar to that of (Yb:Y)AG, the large absorption coefficient of (Yb:Y)AP predicts the usability of (Yb:Y)AP as an RBL medium because the small-signal gain is proportional to the absorption coefficient. Figure 4 presents the calculated absorption coefficient and the small-signal gain γ using equation (6) as a function of the wavelength of (Yb:Y)AG excited at 1030 nm (E3→E5) and (Yb:Y)AP excited at 1018 nm (E4→E6). At these excitation wavelengths, both materials under ideal conditions work as RBL medium because these pump wavelengths at 1030 and 1018 nm were longer than their mean fluorescence wavelengths as predicted in Fig. 3(a,b). The solid curve shows the obtained small-signal gain spectrum and the region where $\gamma > 0$ is yellow filled. The dashed curve indicates the absorption spectra converted from the measured luminescence spectra by McCumber's relationship[25] which is available nearby room temperature in RE-doped material[26]. Besides, the typical absolute absorption coefficients[27], energy levels, fluorescence lifetimes[28,29], and crystal structures[19] of (Yb:Y)AP and (Yb:Y)AG single crystals that Yb-doping concentrations are similar with ours were referenced from some literature for this calculation.

According to the small-signal gain spectra shown in Fig. 4(a,b), (Yb:Y)AP has the maximum gain of 0.27 cm^{-1} at 1041.3 nm which is 3.5 times larger than that of 0.078 cm^{-1} in (Yb:Y)AG at 1049.7 nm. The high small-signal gain of (Yb:Y)AP is arising from not only the large absorption coefficient of (Yb:Y)AP, but also its intrinsic energy structure showing the wider energy difference between pump and lasing energy compared with that of (Yb:Y)AG. Our calculation results indicate the usability of (Yb:Y)AP as an RBL material and the small-signal gain of RBL material utilizing an *f-f* transition of RE-dopant can be controlled by engineering the surrounding crystal fields of the RE-dopant.

Figure 4(c) shows the temperature-dependent small-signal gain of (Yb:Y)AG and (Yb:Y)AP under same pump condition as above (Figure (a,b)) from 250 to 350 K. Note that the absolute absorption coefficient at 300 K was referred although the oscillator strength of intra-orbital transition of shielded 4f electron in rare-earth element has a small temperature dependence. The calculated temperature dependence of small-signal gain shows more low temperature more large gain can be achieved. For example, in (Yb:Y)AP at 250 K, the small-signal gain of 0.38 cm−1 is attainable which is 1.39 times larger than that at 300 K. This result suggests that improving cooling efficiency also develops the output power of RBL well.

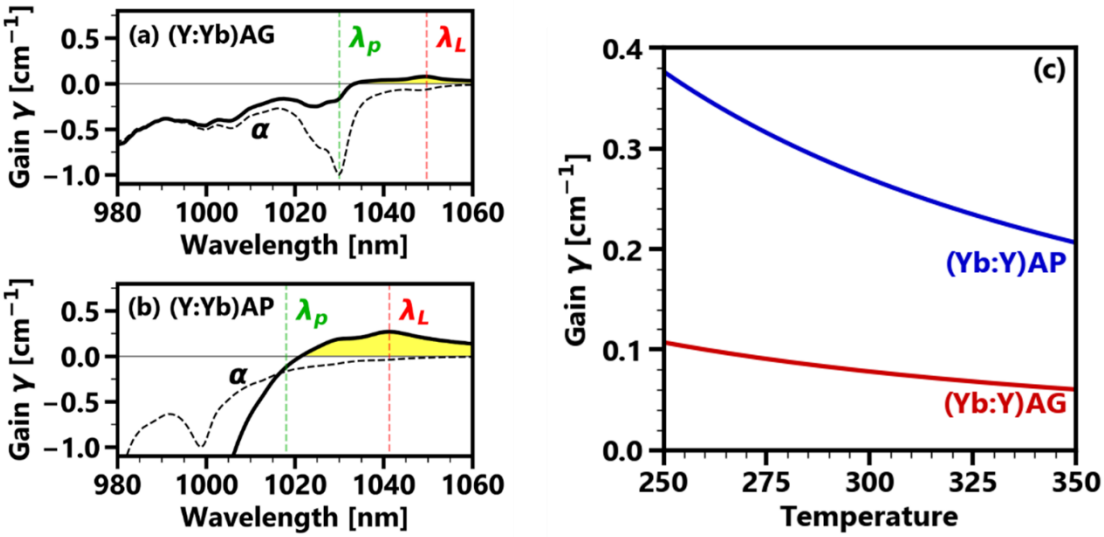

Figure 4 The laser gain of (a) (Yb:Y)AG and (b) (Yb:Y)AP operating as a radiation balanced laser under the condition of i_p=6, I_L=0, and T=300 K. Where, the λ_P is the pump wavelength, λ_L is the lasing wavelength. The pump wavelengths for (Yb:Y)AG and (Yb:Y)AP are 1030 and 1018 nm, respectively. (c) Temperature-dependent small-signal gain of (Yb:Y)AG and (Yb:Y)AP under same pump condition as (a,b). Note that the absolute absorption coefficient at 300 K was referred to although the oscillator strength of intra-orbital transition of shielded 4f electron in rare-earth element has a small temperature dependence.

4. CONCLUSION

A laser cooling in oxides by more than 8.8 K and a larger RBL gain in Yb:YAP can be anticipated due to the low multi-phonon relaxation probability of Yb:YAP. In this work, we fabricated (Yb:Y)AP ceramics by solid-state reaction method and carried out the PL measurement under indirect excitation, the anti-Stokes PL measurement with direct excitation, the PLE imaging, a calculation of the ideal cooling efficiency, and the RBL gain, and compared with those of (Yb:Y)AG. The comparable ideal cooling efficiency of (Yb:Y)AP with that of (Yb:Y)AG estimated by the spectroscopic way is consistent with the ideal cooling efficiency of Yb-doped materials previously predicted. On the other hand, due to the strong absorption and the energy structure, (Yb:Y)AP shows the large small-signal gain as RBL material which is 3.5 times higher than that of (Yb:Y)AG. Our calculation results indicate the usability of (Yb:Y)AP as an RBL material and the small-signal gain of RBL material utilizing an *f-f* transition of RE-dopant can be controlled by engineering the surrounding crystal fields of the RE-dopant.

REFERENCE

[1] Pringsheim, P., "Zwei Bemerkungen über den Unterschied von Lumineszenz- und Temperaturstrahlung," Zeitschrift für Phys. **57**(11–12), 739–746 (1929).

[2] Kushida, T. and Geusic, J. E., "Optical refrigeration in Nd-doped yttrium aluminum garnet," Phys. Rev. Lett. **21**(16), 1172–1175 (1968).

[3] Melgaard, S., Seletskiy, D., Polyak, V., Asmerom, Y. and Sheik-Bahae, M., "Identification of parasitic losses in Yb:YLF and prospects for optical refrigeration down to 80K," Opt. Express **22**(7), 7756–7764 (2014).

[4] Melgaard, S. D., Albrecht, A. R., Hehlen, M. P. and Sheik-Bahae, M., "Solid-state optical refrigeration to sub-100 Kelvin regime," Sci. Rep. **6**(20380), 20380-1–6 (2016).

[5] Hehlen, M. P., Meng, J., Albrecht, A. R., Lee, E. R., Gragossian, A., Love, S. P., Hamilton, Ch. E., Epstein, R. I. and Sheik-Bahae, M., "First demonstration of an all solid-state optical cryocooler," Light Sci. Appl. **7**(15), 1–10 (2018).

[6] Yang, Z., Meng, J., Albrecht, A. R. and Sheik-Bahae, M., "Radiation-balanced Yb : YAG disk laser," Opt. Express **27**(2), 1392–1400 (2019).

[7] Rupper, G., Kwong, N. H. and Binder, R., "Large excitonic enhancement of optical refrigeration in semiconductors," Phys. Rev. Lett. **97**(117401), 117401-1–4 (2006).

[8] Zhang, S., Zhukovskyi, M., Jankó, B. and Kuno, M., "Progress in laser cooling semiconductor nanocrystals and nanostructures," NPG Asia Mater. **11**(54), 1–19 (2019).

[9] Zhang, S., Zhang, Z., Zhukovskyi, M., Jankó, B. and Kuno, M., "Up-conversion emission thermometry for semiconductor laser cooling," J. Lumin. **222**(117088), 1–5 (2020).

[10] Riseberg, L. A. and Moos, H. W., "Multiphonon orbit-lattice relaxation of excited states of rare-earth ions in crystals," Phys. Rev. **174**(2), 429–438 (1968).

[11] Miniscalco, W., "Optical and Electronic Properties of Rare Earth Ions in Glasses," [Rare-earth doped fiber lasers and amplifiers], M. J. F. Digonnet, Ed., Mrcel Dekker, Inc, 29–33 (2001).

[12] Dijk, J. M. F. van and Schuurmans, M. F. H., "On the nonradiative and radiative decay rates and a modified exponential energy gap law for 4f-4f transitions in rare-earth ions," J. Chem. Phys. **78**(9), 5317–5323 (1983).

[13] Zhang, X. X., Schulte, A. and Chai, B. H. T., "Raman spectroscopic evidence for isomorphous structure of GdLiF4 and $YLiF_4$ laser crystals," Solid State Commun. **89**(2), 181–184 (1994).

[14] Dieke, G. H. and Crosswhite, H. M., "The Spectra of the Doubly and Triply Ionized Rare Earths," Appl. Opt. **2**(7), 675–686 (1963).

[15] Bowman, S. R., "Lasers without internal heat generation," IEEE J. Quantum Electron. **35**(1), 115–122 (1999).

[16] Epstein, R. I., Brown, J. J., Edwards, B. C. and Gibbs, A., "Measurements of optical refrigeration in ytterbium-doped crystals," J. Appl. Phys. **90**(9), 4815–4819 (2001).

[17] Suda, J., Kamishima, O., Hamaoka, K., Matsubara, I., Hattori, T. and Sato, T., "The first-order raman spectra and lattice dynamics for $YAlO_3$ crystal," J. Phys. Soc. Japan **72**(6), 1418–1422 (2003).

[18] Chen, Y. F., Lim, P. K., Lim, S. J., Yang, Y. J., Hu, L. J., Chiang, H. P. and Tse, W. S., "Raman scattering investigation of Yb: YAG crystals grown by the Czochralski method," J. Raman Spectrosc. **34**(11), 882–885 (2003).

[19] Zhan, X., Li, Z., Liu, B., Wang, J., Zhou, Y. and Hu, Z., "Theoretical Prediction of Elastic Stiffness and Minimum Lattice Thermal Conductivity of $Y_3Al_5O_{12}$, $YAlO_3$ and $Y_4Al_2O_9$," J. Am. Ceram. Soc. **95**(4), 1429–1434 (2012).

[20] Rydberg, S. and Engholm, M., "Charge transfer processes and ultraviolet induced absorption in Yb:YAG single crystal laser materials," J. Appl. Phys. **113**(223510), 223510-1–6 (2013).

[21] Epstein, R. I. and Sheik-Bahae, M., "Optical Refrigeration in Solids: Fundamentals and Overview," [Optical Refrigeration: Science and Applications of Laser Cooling of Solids], WILEY-VCH Verlag GmbH & Co., 1–32 (2009).

[22] Zeng, X., Zhao, G., Xu, X., Li, H., Xu, J., Zhao, Z., He, X., Pang, H., Jie, M. and Yan, C., "Comparison of spectroscopic parameters of 15 at% Yb:$YAlO_3$ and 15 at% Yb:$Y_3Al_5O_{12}$," J. Cryst. Growth **274**, 106–112 (2005).

[23] Nakayama, Y., Harada, Y. and Kita, T., "Improving laser cooling efficiencies of Yb-doped yttrium aluminum garnet by utilizing non-resonant anti-Stokes emission at high temperatures," Opt. Express **27**(24), 34961–34973 (2019).

[24] Balliu, E., Thontakudi, A., Knall, J. M. and Digonnet, M. J. F., "Predictive comparison of anti-Stokes fluorescence cooling in oxide and non-oxide fiber hosts doped with Er^{3+} or Yb^{3+}," Proc. SPIE **10936**(109360J), 109360J-1–7 (2019).

[25] McCumber, D. E., "Einstein relations connecting broadband emission and absorption spectra," Phys. Rev. **136**(4A), 16–19 (1964).

[26] Quimby, R. S., "Range of validity of McCumber theory in relating absorption and emission cross sections," J. Appl. Phys. **92**(1), 180–187 (2002).

[27] Wang, X., Xu, X., Zhao, Z., Jiang, B., Xu, J., Zhao, G., Deng, P., Bourdet, G. and Chanteloup, J. C., "Comparison of fluorescence spectra of Yb:$Y_3Al_5O_{12}$ and Yb:$YAlO_3$ single crystals," Opt. Mater. (Amst). **29**(12), 1662–1666 (2007).

[28] Boulon, G., Guyot, Y., Canibano, H., Hraiech, S. and Yoshikawa, A., "Characterization and comparison of Yb^{3+}-doped $YAlO_3$ perovskite crystals (Yb:YAP) with Yb^{3+}-doped $Y_3Al_5O_{12}$ garnet crystals (Yb:YAG) for laser application," J. Opt. Soc. Am. B **25**(5), 884 (2008).

[29] Patel, F. D., Honea, E. C., Speth, J., Payne, S. A., Hutcheson, R. and Equall, R., "Laser demonstration of $Yb_3Al_5O_{12}$ (YbAG) and materials properties of highly doped Yb:YAG," IEEE J. Quantum Electron. **37**(1), 135–144 (2001).